nature
cell biology

Genome-scale RNAi profiling of cell division in human tissue culture cells

Ralf Kittler[1,6], Laurence Pelletier[1,7], Anne-Kristine Heninger[1], Mikolaj Slabicki[1], Mirko Theis[1], Lukasz Miroslaw[1], Ina Poser[1], Steffen Lawo[7], Hannes Grabner[1,2], Karol Kozak[1,2], Jan Wagner[1,2], Vineeth Surendranath[1], Constance Richter[1], Wayne Bowen[3], Aimee L. Jackson[4], Bianca Habermann[1,5], Anthony A. Hyman[1] and Frank Buchholz[1,8]

Cell division is fundamental for all organisms. Here we report a genome-scale RNA-mediated interference screen in HeLa cells designed to identify human genes that are important for cell division. We have used a library of endoribonuclease-prepared short interfering RNAs for gene silencing and have used DNA content analysis to identify genes that induced cell cycle arrest or altered ploidy on silencing. Validation and secondary assays were performed to generate a nine-parameter loss-of-function phenoprint for each of the genes. These phenotypic signatures allowed the assignment of genes to specific functional classes by combining hierarchical clustering, cross-species analysis and proteomic data mining. We highlight the richness of our dataset by ascribing novel functions to genes in mitosis and cytokinesis. In particular, we identify two evolutionarily conserved transcriptional regulatory networks that govern cytokinesis. Our work provides an experimental framework from which the systematic analysis of novel genes necessary for cell division in human cells can begin.

The use of RNA-mediated interference (RNAi) for gene silencing has provided a powerful tool for loss-of-function studies in a variety of metazoans[1]. In combination with high-throughput assays, genome-wide RNAi studies in invertebrates have uncovered novel gene functions in various biological processes[2]. Several of these studies were aimed at the identification of genes essential for cell division and cell cycle progression in *Caenorhabditis elegans* and cultured *Drosophila* cells[3–7]. Because defective regulation of cell division provokes human disease, particularly leukaemias and other cancers[8–10], a global survey of genes essential for cell division in human cells would not only advance the understanding of a fundamental biological process but may also deliver novel diagnostic and therapeutic targets for cancer.

We and others have developed endoribonuclease-prepared short interfering RNAs (esiRNAs) as potent and specific mediators of RNAi[11] in mammalian cells. We previously conducted a proof-of-concept screen validating the use of esiRNAs for the identification of genes required for cell division in HeLa cells[12]. The use of highly complex pools of siRNAs decreases off-target effects[13], which have been recognized as a major hurdle in RNAi screens[14–16].

Here we use an improved esiRNA library with genome-scale coverage[13]. We performed high-throughput DNA content analysis for the initial detection of cell cycle arrest and altered ploidy phenotypes, which were further analysed by fluorescence imaging, flow cytometry and time-lapse video microscopy. Using hierarchical clustering we grouped the identified genes on the basis of their multiparameter signatures into phenotypic classes, as a prelude for more detailed bioinformatic and functional analyses of their specific functions in mitosis and cytokinesis. Using this approach we uncovered a multitude of new genes implicated in these processes, including two evolutionarily conserved transcriptional regulatory networks that govern cytokinesis in mammalian cells.

RESULTS
Primary screen and validation
To identify cell division genes in HeLa cells, we developed a rapid and robust DNA content assay amenable to the high-throughput detection of phenotypes induced by RNAi (Fig. 1). We used an esiRNA library targeting 17,828 genes (Supplementary Information, Table S1) to transfect the cells and stained chromatin with propidium iodide 72 h after transfection. The DNA content histograms obtained were analysed and scored as a hit when a distance with a highly significant difference (more than 3 s.d.) from that of the negative controls was observed. Using these criteria we nominated 2,146 genes that altered cell cycle progression or ploidy on knockdown (Fig. 1, and Supplementary Information, Table S1).

**Genome-scale human esiRNA library
targeting 17,828 genes**

Primary screen → Transfection of HeLa cells

DNA content analysis
(*laser scanning cytometry*)

Control   Phenotype

2146 primary hits

Verify gene expression in
HeLa cells (RT–PCR)

Synthesize secondary
esiRNA library

1726 hits subjected to secondary screening

Transfection

Repeat DNA content analysis

Secondary screen

Measure cell size (flow cytometry)

Measure mitotic index (imaging)

Control   Phenotype

**Nine-parameter fingerprint of 1351 genes
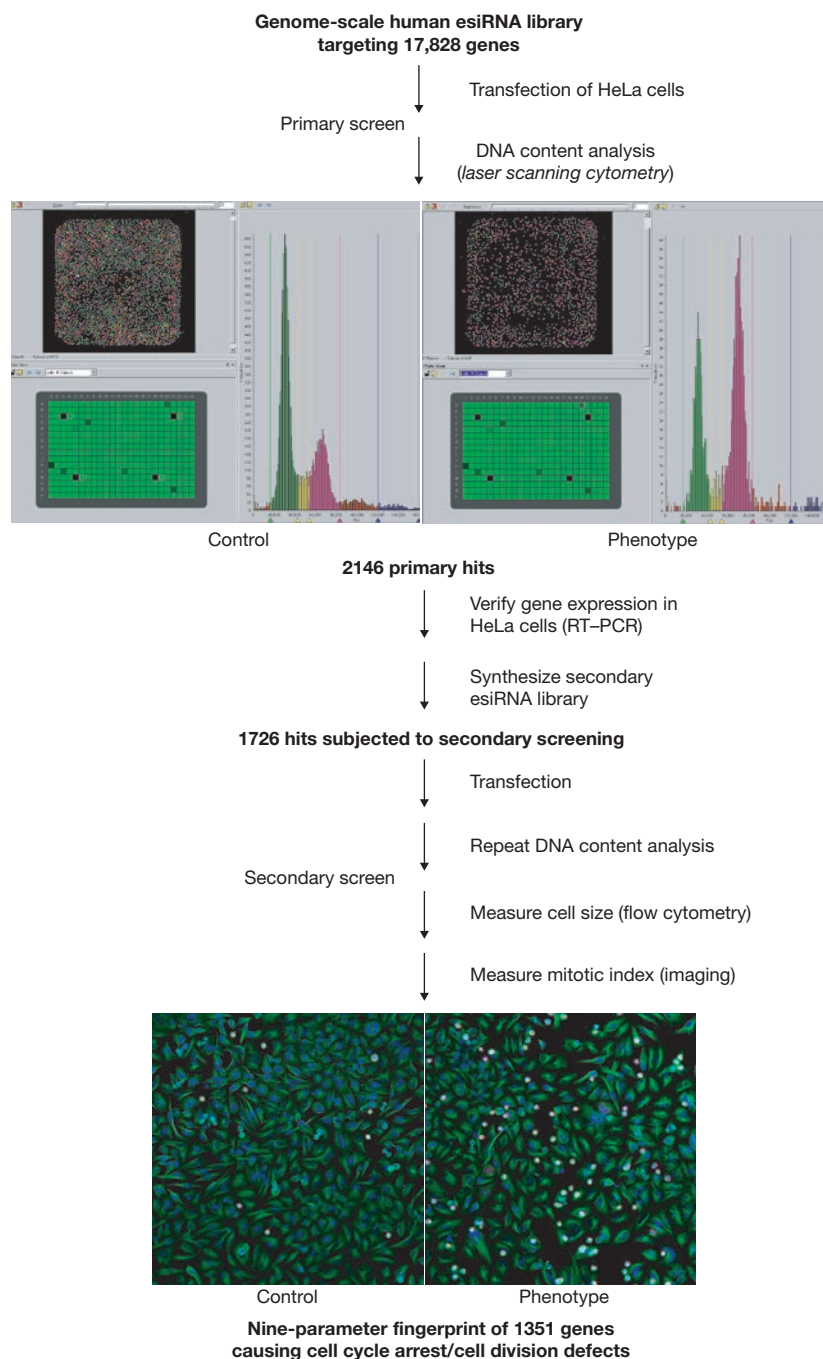causing cell cycle arrest/cell division defects**

Figure 1 Screening strategy. Flow diagram of the genome-scale screening strategy for genes essential for cell cycle progression in human cells. Important steps are shown.

High-throughput screens typically produce false positives due to experimental errors. In addition, RNAi screens can contain false positives due to off-target effects[14–16]. To minimize the number of false positives in our screen we developed a three-step validation protocol. First, we analysed the expression status of the primary hits in HeLa cells; second, we resynthesized the esiRNAs and repeated the DNA content analysis for the genes that passed the first valida-tion step. Third, we generated and assayed a second non-overlapping esiRNA for the genes that passed the second validation step. This cumulative validation procedure ensures that the data set we present is of high quality (for details on the hit validation see Methods and Supplementary Methods).

A second important aspect for assessing the quality of our RNAi data set is the evaluation of the rate of false negatives, which is an indicator for the saturation level of the screen. We used the analyses of subunit coverage for protein complexes/pathways to test screening efficiency (Supplementary Information, Table S2). This analysis indicated an overall high degree of efficiency (72%) for our screen, although the

Table 1 Overlap between RNAi screens

	Overlap (percentage)			
	H. sapiens (this study)	*H. sapiens*[27]	*D. melanogaster*[3]	*C. elegans*[7]
H. sapiens (this study)	–			
H. sapiens[27]	10	–		
D. melanogaster[3]	38	12	–	
C. elegans[7]	36	10	ND	–

For two human cell lines the overlap was calculated as the percentage from the putative human orthologues of genes that scored in the fly and in the worm RNAi screens. ND, not determined.

detection rate varied between 31% and 100% for individual complexes, which probably reflects differences in the stability of the corresponding complex subunits (for details on the evaluation of the rate of false negatives see Supplementary Methods).

Secondary screen and profile analysis of RNAi phenotypes

We extracted seven parameters from the DNA content analyses of the 1,351 hits that passed the second validation step: G1, S, G2/M, 8*N* (polyploid) DNA content, cell number, the percentage of dead cells and debris (subG1; that is, a DNA content of less than 2*N*) and the percentage of cells with 4*N*–8*N* DNA, which provided a measure for aneuploidy (Fig. 2a, b). We performed two additional assays to further characterize the cell cycle progression and cell division defects. For the first assay we determined the mitotic index for each hit gene to distinguish between cells in G2 and those in mitotic arrest. For the second assay we determined cell size by flow cytometry as an indicator of cell growth. Reproducibility for all parameters was documented by a linear regression analysis of all duplicate plate pairs, which yielded a high degree of reproducibility for the cell cycle parameters determined (Fig. 2c–h). Our screen therefore allowed the accurate detection and quantification of different types of cell cycle progression and division defects (Fig. 2i–p).

The secondary screen produced a nine-parameter fingerprint for each phenotype. We used these signatures to assign the corresponding genes to functional groups through hierarchical clustering, on the assumption that phenotypic profiles should reflect similar functions. On the basis of the gene clusters obtained (Fig. 3a) and manual inspection, we grouped the genes into four phenotypic classes: G0/G1 arrest, S arrest, G2 arrest, and cell division defects (Supplementary Information, Table S1). To annotate the identified genes we searched for functional data in two databases. We identified 217 genes previously associated with cell cycle progression, and assigned a novel function in cell cycle progression to 252 previously uncharacterized genes (Supplementary Information, Table S1). Furthermore, we identified 882 known genes that had previously been implicated in functions other than cell cycle progression and cell division. We grouped the hit genes into 12 functional categories (Supplementary Information, Table S1) that included processes relevant for cell cycle regulation such as transcriptional regulation, protein (de)ubiquitination and protein (de)phosphorylation.

We tested the reliability of phenotype grouping by searching our hit list for known cell cycle regulators and found many of them in the expected cluster (Fig. 3a). More than 50% (721) of all detected phenotypes (Fig. 3b) led to an increase in the number of cells with 2*N* DNA content, suggestive of either G1 arrests or exit from the cell cycle into G0. This phenotypic class contained known regulators for G1/S transition such as *CCNE1*, *MYC*, *E2F* and *TFDP1*. RNAi-mediated knockdown of 157 genes with a G0/G1 arrest caused a decrease in cell size indicative

of impaired growth, whereas RNAi of 93 genes led to an increase in cell size, which may reflect a primary defect in G1/S transition. Similarly, we detected among the G2 arrest phenotypes the key regulator for G2/M transition, *CDC2* (*CDK1*). The S arrest cluster contained many known genes implicated in DNA replication (such as *CDC45L*, *PCNA* and those encoding replication protein A subunits and DNA polymerases) and dNTP synthesis (such as *RRM1* and *RRM2*). A delay in S phase was also observed for the knockdown of histones and genes that are implicated in histone expression (such as *SLBP* and *NPAT*) and chromatin assembly (such as *CHAF1A*). This finding may reflect the tight coordination of histone and DNA synthesis that is necessary for the proper replication of chromatin[17,18]. The cell division phenotypes contained a wealth of known regulators of mitosis and cytokinesis, for example *PLK1*, *KIF11*, *CDC20*, *ESPL1* (Separase), *SGOL1* (Shugoshin), *CDCA5* (Sororin), *CENPE*, *KNTC2* (Hec), *STK6* (Aurora A), *ch-TOG*, *TPX2*, *AURKB* (Aurora B), *INCENP*, *ANLN* (Anillin), *RACGAP1* (MgcRacGAP), *ECT2*, *PRC1* and *KIF23* (MKLP-1).

The congruence of genes with known cell cycle and cell division functions with the four phenotypic classes indicates that these clusters indeed reflect specific processes. We can therefore propose functions for uncharacterized genes by analysing their phenotypic profiles. For example, the silencing of genes implicated in DNA replication caused a delay in S phase. It is therefore plausible to assume similar functions for previously uncharacterized genes with the same phenotypic profile. For example, BLAST analysis of the predicted gene C17ORF41, which resulted in a pronounced S-phase delay, revealed weak protein sequence similarity ($E = 5 \times 10^{-14}$) to *RFC1* (encoding replication factor C1). RFC1 is essential for the loading of proliferating-cell nuclear antigen (PCNA) onto the 3′ ends of primer DNA to form a DNA sliding clamp that keeps DNA polymerase engaged at the replication fork[19]. Strikingly, *PCNA* was identified as the closest phenotypic profile neighbour of C17ORF41 (Fig. 3c). Although a weak sequence similarity of C17ORF41 to *RFC1* alone would be insufficient for functional annotation, in combination with RNAi profiling it enables us to assign a function for C17ORF41 in DNA replication with high confidence, potentially as a DNA clamp loader.

High-resolution analysis of cell division phenotypes

We selected the genes for which cluster analysis suggested a role in cell division for a more detailed functional characterization. Of these 289 genes, 223 caused an altered ploidy on knockdown. These genes may have special relevance for cancer biology, considering that genome instability and altered ploidy have been implicated in tumorigenesis[10,20].

In general, there are two major events that lead to altered ploidy. These are mitotic defects that impair spindle assembly and chromosome segregation, and cytokinesis defects preventing the proper division of the cytoplasm. We first analysed the phenotypic profiles of three well-known

mitotic and cytokinesis regulators (Fig. 4a–d) and used these signatures as core patterns to group the 223 genes into a cytokinesis defect cluster of 131 genes and a mitotic defect cluster of 92 genes (Fig. 4e–f, and Supplementary Information, Table S3). To evaluate the reliability of this grouping we analysed randomly 68 phenotypes by video microscopy of a HeLa cell line stably expressing histone–GFP (green fluorescent protein). Of the predicted mitotic defects, 91% showed defects in prometaphase or metaphase (in most cases accompanied by an arrest in these phases) from which some cells exited with unequal or no chromosome segregation. Of the predicted cytokinesis defects, 96% showed normal progression through mitosis until telophase, when the cells failed to divide the cytoplasm (Supplementary Information, Table S3). Thus, we can distinguish between gene functions in chromosome segregation and cytokinesis with high confidence by phenotypic profiling. For 184 genes, bioinformatic analyses revealed novel functions in cytokinesis or mitosis (Supplementary Information, Table S3).

Because defects in spindle assembly and cytokinesis have been linked to aneuploidy and cancer progression, we searched the literature for the 223 genes causing altered ploidy on knockdown and found that 51 (23%) of them had putative roles in tumorigenesis (Supplementary Information, Table S3). We analysed one of these genes, *CASC5*, in more detail because of its striking RNAi phenotype. *CASC5* is a fusion partner of the *MLL* oncogene in acute lymphoblastic leukaemia and is upregulated in certain types of lung cancer[21–23]. Knockdown of *CASC5* resulted in a severe chromosome congression defect leading to an unequal distribution of chromosomes to daughter cells (Fig. 5e–h, and Supplementary Information, Movie S1). The cells also progressed significantly faster through mitosis (Fig. 5i) and showed a marked decrease in the spindle checkpoint proteins Bub1 and BubR1 at the kinetochores of prometaphase cells (Fig. 5j–u). This phenotype is consistent with a defect in kinetochore function, which impairs both microtubule capture and the activation of the spindle assembly checkpoint. Interestingly, *CASC5* was recently identified in two proteomic studies as a component of the human kinetochore (as KIAA1570 and AF15q14) and was suggested to be the putative orthologue of the *KNL-1* gene in *C. elegans* and *Spc105* in *Saccharomyces cerevisiae*[24,25]. The *C. elegans* orthologue is required for the targeting of multiple components of the outer kinetochore, which is consistent with a 'kinetochore-null' phenotype observed on RNAi-mediated knockdown[26]. The loss-of-function phenotype we now report therefore shows that human *CASC5* is an essential component of the mammalian kinetochore. Because of the severe chromosome segregation defect and the inactivation of the spindle checkpoint on knockdown, we speculate that *CASC5* has a role in early tumorigenesis by causing aneuploidy.

Cross-species RNAi comparisons

Genome-wide data sets for cell cycle progression and/or cell division have previously been reported for *C. elegans* and cultured *Drosophila* cells[3,7]. We combined these results with data for human tissue culture cells presented here on HeLa cells and for U2OS cells[27] for a cross-species comparison of requirements for cell division. Although all four screens are not saturating (Supplementary Information, Table S2) and some of the genes of these data sets might have a different function or have become genetically redundant in different lineages, a cross-species comparison of cell cycle/cell division data should enable the identification of conserved regulatory pathways and functional modules.

We first analysed the global overlap between the screens and found that 38% of the fly genes and 36% of the worm genes with clear human orthologues were also identified in our screen (Table 1, and Supplementary Information, Table S4). These genes are therefore likely to have highly conserved gene functions in the cell cycle and cell division and to encode proteins with a high degree of sequence conservation. Second, we performed a more detailed cross-species analysis of cytokinesis defects, because for this phenotypic class the data source for cross-species comparisons is the largest available[3–5,28]. We compared these data sets with our screening data to identify conserved regulatory pathways for cytokinesis. This analysis revealed numerous motor proteins and central spindle components, confirming the conserved role of these proteins in cytokinesis (Supplementary Information, Table S4).

Identification of conserved transcriptional regulators for cytokinesis

Interestingly, the cross-species comparison of cytokinesis genes yielded genes encoding putative chromatin-binding proteins implicated in transcriptional repression. The knockdown of *NCOR2*, which is a co-repressor of various transcription factors[29] resulted in a cytokinesis defect (Supplementary Information, Movie S2). A similar phenotype was reported for the *D. melanogaster* homologue *Smr*[4] reflecting a high degree of functional conservation of *NCOR2* in cytokinesis. The analysis of *NCOR2* profile neighbours suggested functional interaction with *TBL1X* and *MLL5* (Fig. 3d). Bioinformatic analyses identified three putative *S. cerevisiae* homologues, *SNT1* (*NCOR2*), *SET3* (*MLL5*) and *SIF2* (*TBL1X*), encoding proteins that form the histone deacetylase-recruiting SET3 complex (SET3C) for the repression of meiosis-specific genes, including cytokinesis genes[30]. Strikingly, NCOR2 was recently found to interact with TBL1X and MLL5 in nuclear extracts of HeLa cells, substantiating the existence of a human SET3 complex (www.nursa.org/10.1621/datasets.01002). On the basis of these findings we propose a human SET3 complex composed of the NCOR2, MLL5 and TBL1X proteins (Fig. 3e), which might regulate either the expression of genes involved in cytokinesis or the chromatin structure of mitotic chromosomes.

We also identified a putative transcriptional regulatory complex containing the protein DKFZp686L1814 (LIN54). The silencing of the corresponding gene caused cytokinesis defects (Fig. 6a, b, and Supplementary Information, Movie S3) and a weak mitotic arrest (Supplementary Information, Table S1). We used the cross-species RNAi rescue approach[31] to confirm the role of *LIN54* in cytokinesis (Fig. 6e, f) and to show that GFP-tagged LIN54 protein localizes to the nucleus, which is consistent with its role in transcriptional regulation (Fig. 6c, d). A cross-species comparison revealed that the putative *D. melanogaster* orthologue *MIP120* is a component of the dREAM complex (*Drosophila* RBF, E2F2 and Myb interacting proteins containing complex)[32,33], whereas the *C. elegans Lin-54* is a component of the DRM complex (DP, Rb and MuvB containing complex)[34]. The dREAM and DRM complexes have been implicated in regulating Rb/E2F target genes[32–34], many of which are cell cycle-related genes, including genes implicated in cytokinesis, in both *Drosophila* and human cells[35,36]. Furthermore, we found that *Arabidopsis thaliana Tso1*, which has previously been shown to be essential for cytokinesis[37], shares similarity to human *LIN54*. A previous study has shown a role of some dREAM complex subunits in DNA replication in *Drosophila*[38]. To determine whether the cell division defects observed
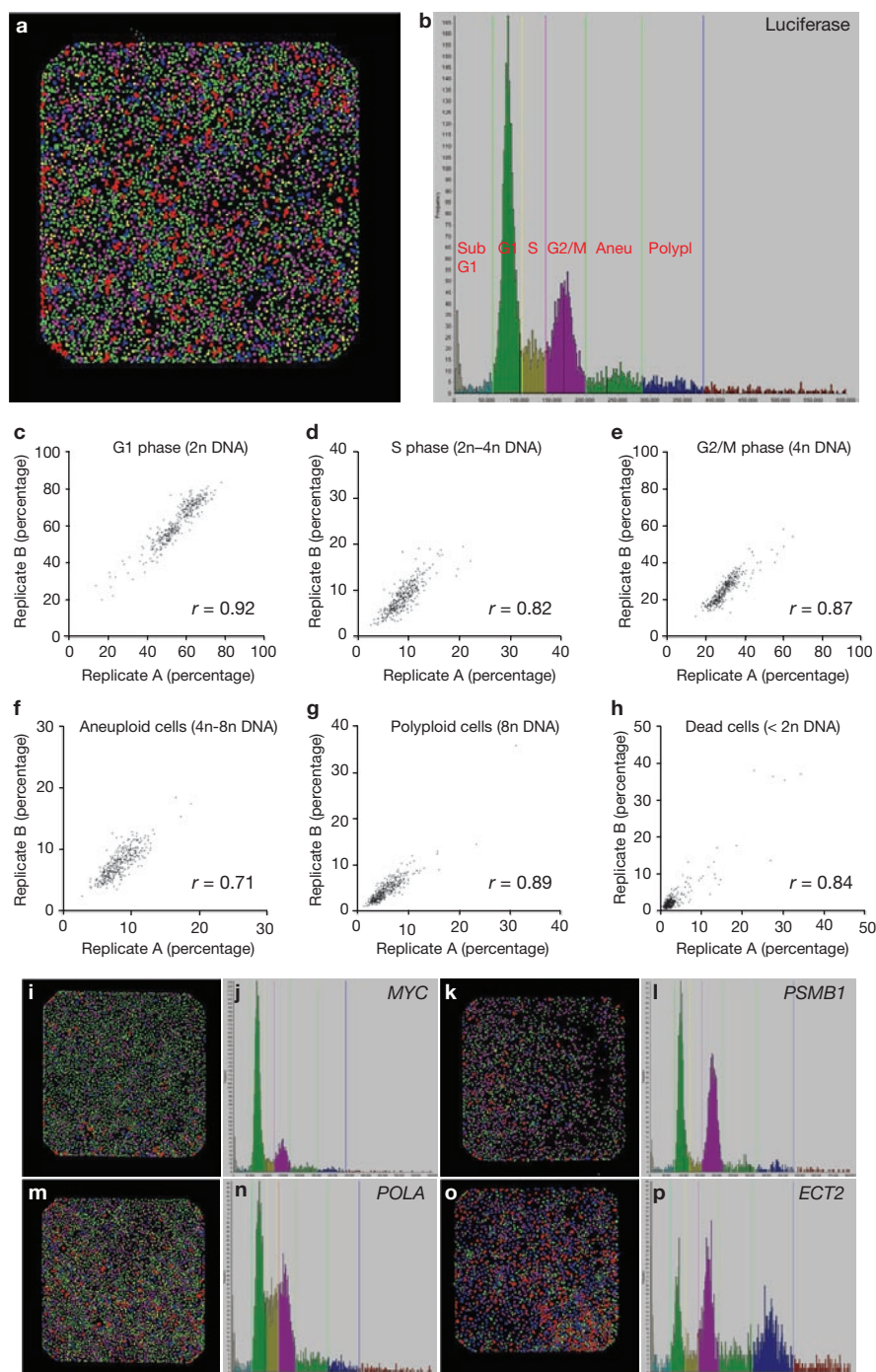
Figure 2 High-throughput detection and reproducibility of cell cycle parameters by DNA content analysis. (**a**) Propidium-iodide-stained nuclei of cells in a single well of a 384-well plate were analysed by laser scanning cytometry 72 h after transfection with control esiRNA targeting firefly luciferase. (**b**) Fluorescence intensities were plotted in a DNA-content histogram and used for gating of indicated cell cycle populations. (**c–h**) Scatter plots of a replicate 384-well plate pair for the percentages of DNA content of G1-phase (**c**), S-phase (**d**), G2/M-phase (**e**), aneuploid (**f**), polyploid (**g**) and dead (**h**) cells. The *r* values indicate the average linear correlation coefficient for replicate plate pairs. (**i–p**) The high reproducibility of DNA content analysis allowed the reliable detection of multiple cell cycle defects, for example G1 arrest (**i**, **j**), G2/M arrest (**k**, **l**), S arrest (**m**, **n**) and accumulation of polyploid cells (**o**, **p**) exemplified by the genes whose names are shown in the DNA content histograms. The reproducibility of the determined cell number, mitotic index and cell size was documented by linear regression analysis as for the other six parameters shown in **c–h**. We determined the following *r* values (indicated in parentheses) for cell number (0.90), mitotic index (0.78) and cell size (0.66). SubG1, debris/dead cells; aneu, aneuploid cells; polypl, polyploid cells.

on LIN54 knockdown were caused indirectly by defective replication, we monitored the dynamics of the key replication protein PCNA in LIN54-depleted cells and control cells (Supplementary Information,

Movies S4 and S5). We did not observe S-phase progression defects on LIN54 depletion, suggesting that the observed cell division defect is not caused by defects in DNA replication. Interestingly, a recent study has
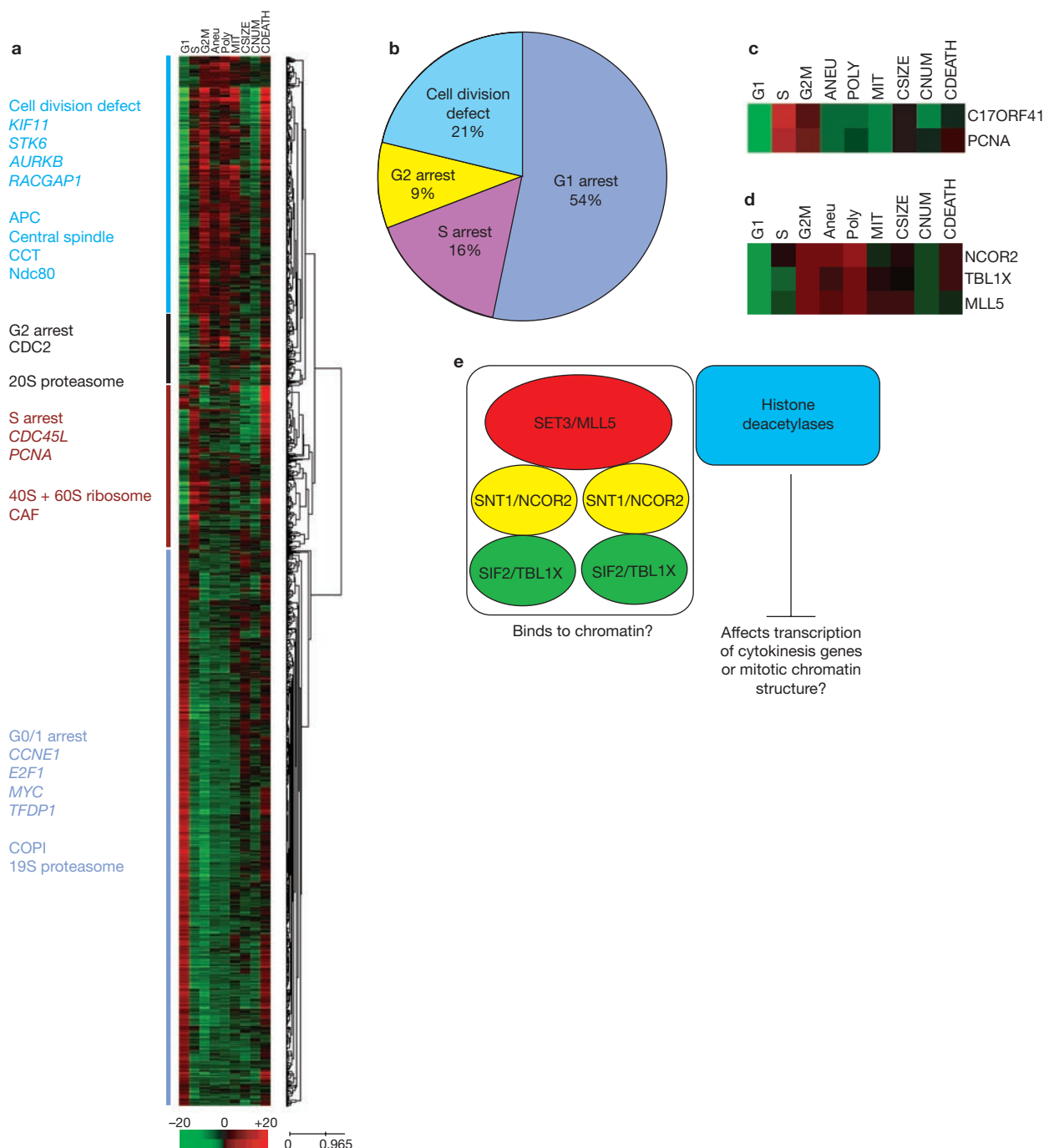
Figure 3 Phenotypic profiling of cell cycle defects. **a**, Hierarchical clustering of cell cycle defects based on their phenotypic signatures. The coloured lines to the left of the heat map indicate the major clusters. The predominantly represented cell cycle defect class is written in the same colour, with example genes of these clusters shown. Exemplified protein complexes for which subunits were found in specific clusters are shown. **b**, Classification of 1,351 cell cycle defects based on hierarchical clustering and subsequent manual inspection. **c**, *PCNA* has the most similar phenotypic profile to C17ORF41, potentially reflecting functional interaction. **d**, Profile analysis of NCOR2, TBL1X and MLL5. Profile comparison between the three genes shown that may indicate functional interaction. **e**, Graphical depiction of the yeast SET3 complex (based on ref. 30) with their predicted human homologues NCOR2, TBL1X and MLL5 form a similar repressor complex like their putative yeast orthologues and a model how this complex regulates the expression of genes implicated in cytokinesis. G2M, G2/M phase; aneu, aneuploidy; poly, polyploidy; MIT, mitotic index; CSIZE, cell size; CNUM, cell number; CDEATH, dead cells; APC, anaphase-promoting complex; CCT, chaperonin-containing T-complex polypeptide 1; Ndc80, Nuf2–Ndc80 complex; CAF, chromatin assembly factor 1; COPI, coatomer I complex.

shown that the human dREAM complex binds to E2F target promoter regions and represses cell-cycle-dependent genes in quiescent T98G cells[39]. If dREAM is a general repressor of cell cycle genes, one might expect that the destruction of the complex would activate the expression of cell cycle genes, somewhat contradicting the observed RNAi phenotype. To test the role of *LIN54* in the transcriptional regulation
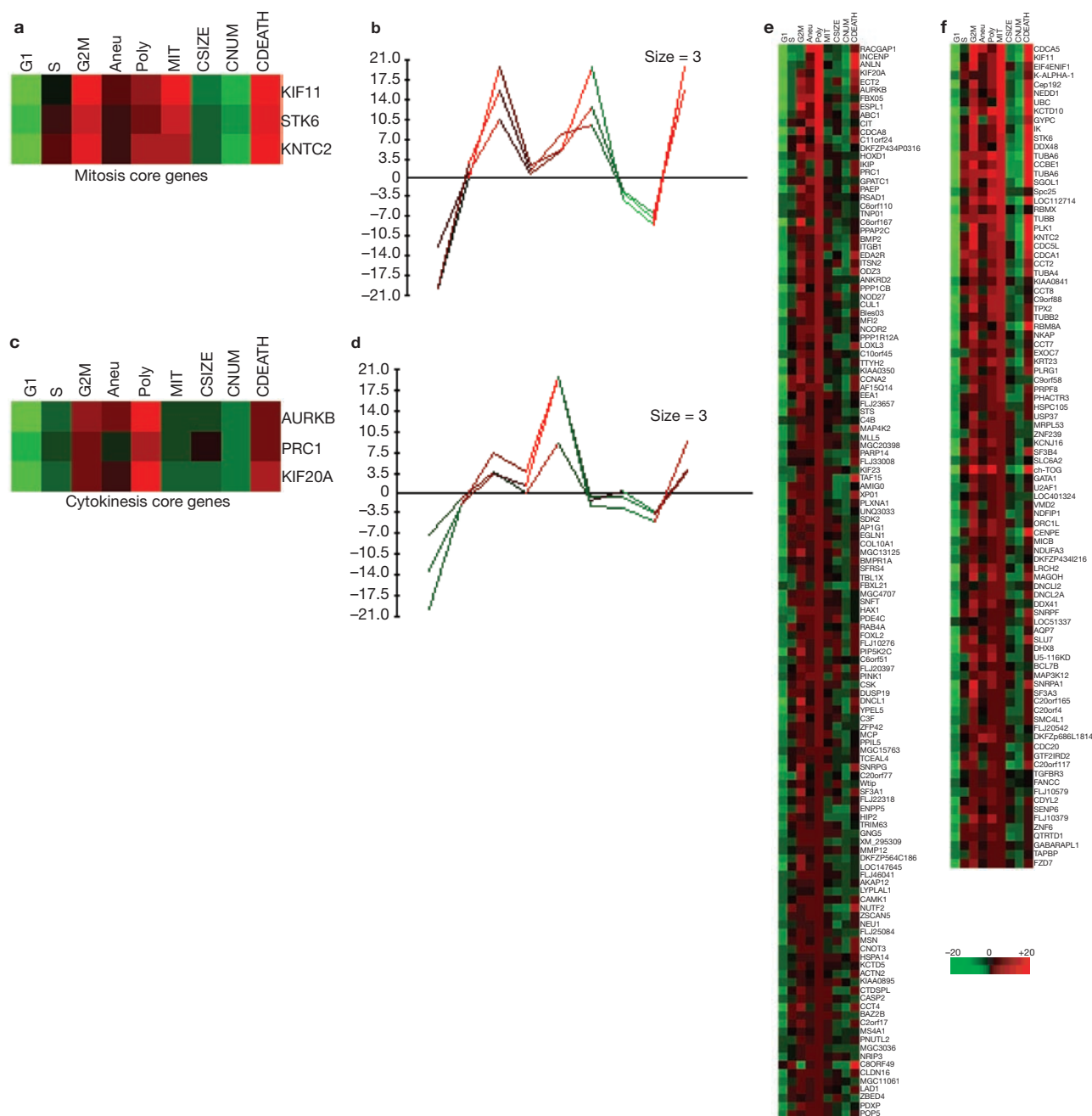
Figure 4 Profile analysis of cell division defects. (**a–d**) Profile comparison between the known mitotic genes *KIF11*, *STK6* and *KNTC2* (**a**, **b**) and the cytokinesis genes *AURKB*, *PRC1* and *KIF20A* (**c**, **d**). (**e**, **f**) On the basis of these core patterns the genes were grouped into a cytokinesis defect cluster (**e**) and a mitosis defect cluster (**f**). Abbreviations in the heat maps are the same as those in Fig. 3.

of cell cycle genes in proliferating cells, we performed gene expression array analyses after LIN54 depletion. Intriguingly, depletion of LIN54 resulted in the downregulation of many cell cycle genes (Fig. 6g, h, and Supplementary Information, Table S5). In particular, genes required for cytokinesis were rapidly downregulated, which is consistent with the observed phenotype. Strikingly, 82% of these genes for which chromatin immunprecipitation data are available[39] showed LIN54 binding in their promoter regions, suggesting that these genes are direct targets of LIN54 (Supplementary Information, Table S5). We tested esiRNAs for two other known subunits of the human dREAM complex (LIN37 and LIN52),

which were not present in the screened esiRNA library. These two esiR-NAs caused a highly significant increase in the 8*N* DNA content, as was observed for LIN54 (Supplementary Information, Table S5). Collectively, these findings indicate that LIN54 acts in a complex that is a transcriptional activator of cell division genes in proliferating cells, in contrast to quiescent cells, in which LIN54 is a transcriptional repressor.

DISCUSSION
Here we used a genome-scale RNAi screening strategy to identify genes required for cell division. Recent reports on the occurrence of false
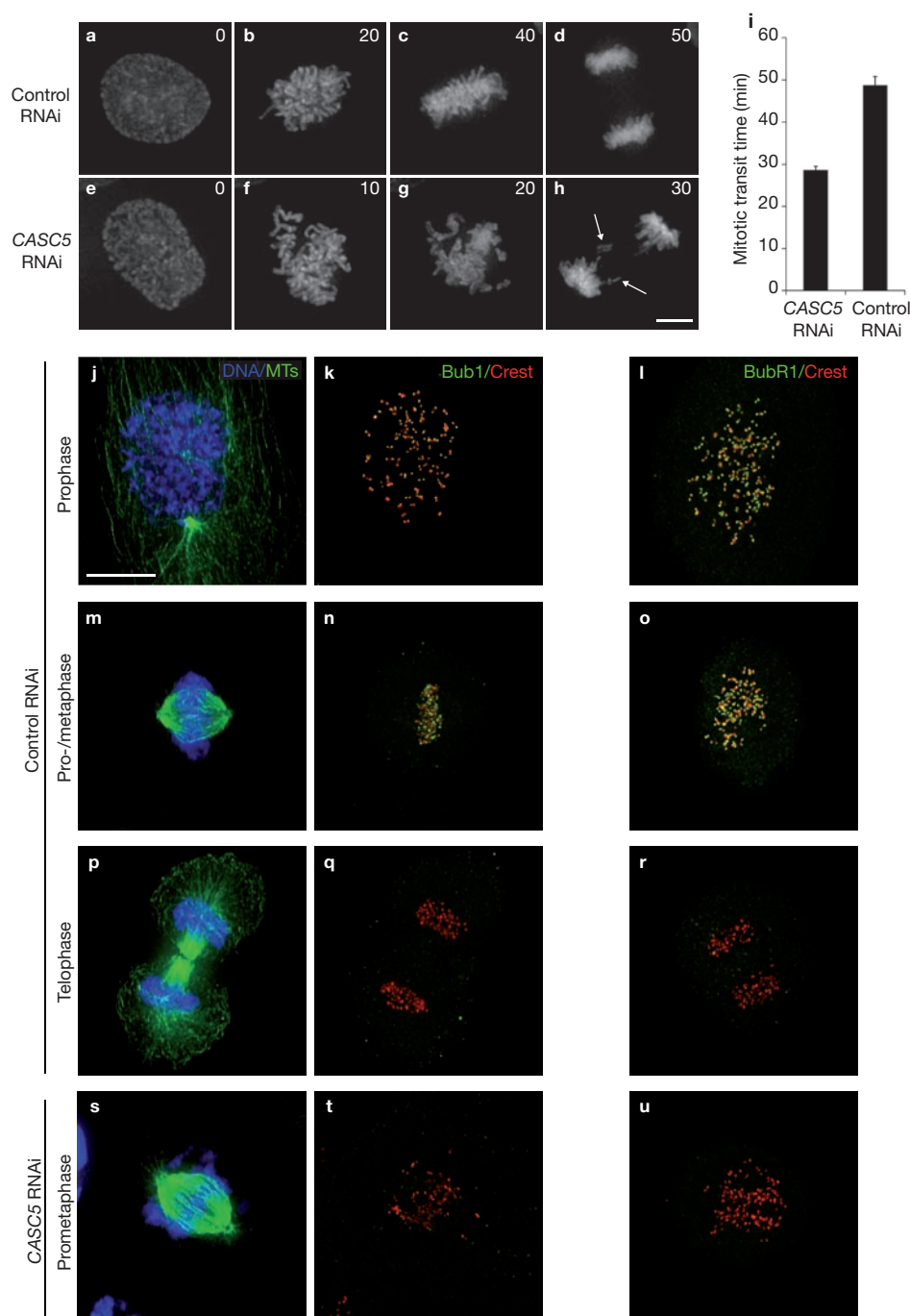
Figure 5 Mitotic phenotype of CASC5 depletion. (**a–h**) High-resolution video microscopy of chromosome dynamics during mitosis in cells transfected with esiRNA targeting firefly luciferase (**a–d**) or *CASC5* (**e–h**). The time-lapse sequence starts 60 h after transfection of a HeLa cell line stably expressing histone–GFP. Numbers indicate minutes after the start of the time-lapse sequence. The arrows in **h** indicate lagging chromosomes. (**i**) Quantification of mitotic transit times from prophase to anaphase for *CASC5* RNAi and control RNAi using esiRNA targeting firefly luciferase. In all, 21 mitoses were analysed for *CASC5* RNAi and 35 for control RNAi, starting 60 h after transfection. Bars indicate means and error bars indicate s.e.m. *P* was calculated as 5×10^{-9} with a two-tailed Mann–Whitney *U*-test. (**j–u**) Loss of Bub1 and BubR1 localization to centromeres on depletion of CASC5. HeLa cells were transfected with esiRNA targeting firefly luciferase and *CASC5*, and were imaged by three-dimensional deconvolution microscopy 48 h after transfection for DNA (blue), microtubules (green), Bub1 (green) or BubR1 (green) and CREST (red). Merged images of DNA/microtubules and of Bub1/CREST and BubR1/CREST at different stages of mitosis in control (**j–r**) and in prometaphase *CASC5* esiRNAi treated cells (**s–u**) are shown. Note that on depletion of CASC5 the checkpoint proteins Bub1 and BubR1 no longer localize to centromeres in prometaphase cells. A total of 50 mitoses of CASC5-depleted cells and control cells were analysed. A loss of centromeric Bub1 localization was observed for 40 and 3 mitoses, and a loss of centromeric BubR1 localization was observed for 39 and 7 mitoses in CASC5-depleted and control cells, respectively. Scale bars, 5 μm (**a–h**); 10 μm (**j–u**).

positives in RNAi screens have raised concerns about the validity of large RNAi data sets[40]. When we compared the genes identified in a recently published siRNA-based screen for cell cycle regulators in human cells[27] with our study, we observed an overlap of only 10% between the two data sets (Table 1). Interestingly, the coverage of protein complex subunits/pathway components and the overlap between the genes identified in mammals and in the fly and worm RNAi screens are lower when using siRNA than when using esiRNA (Table 1, and Supplementary Information, Tables S2 and S4). In the siRNA-based screen, U2OS cells were used in assays similar to those in our study to identify genes required for cell cycle progression. The use of two different cell lines may account for some of the differences in the identified genes required for cell cycle progression or cell division, because many genes implicated in G1 progression and G1/S transition are probably cell-type-dependent (see also below). However, it is unlikely that this divergence alone accounts for all differences because we observed only a slight increase in the overlap rate (from 10% to 12.5%) when we restricted our comparison to genes that resulted in S-phase arrest or cell division defects and were verified by a second esiRNA (Supplementary Information, Table S4). In addition, the comparison with the *C. elegans* and *Drosophila* screens revealed a stronger overlap with our screen. Another possibility would be that the differences observed are caused by the use of different silencing reagents. For our screen we used a well-characterized library of esiRNAs and we carefully validated the genes identified. The characterization of the library revealed a high silencing efficiency and a 12-fold decrease in off-target effects at the mRNA level compared with chemically synthesized siRNA[13]. The high quality of the esiRNA resource translated into a high degree of screening efficiency in this study, as judged by a high saturation rate, and might have avoided many false positives due to off-target effects among the primary hits. The subsequent three-step hit validation eliminated many of the remaining false positives, which ensured an overall high quality of the reported data.

We identified hundreds of genes that on RNAi cause cell cycle arrest and/or cell division defects in HeLa cells. This cell line is the generic experimental system used in many laboratories to study the mammalian cell cycle. As are many other tissue culture cells, HeLa cells are transformed, and it is therefore likely that we have missed genes that are essential in untransformed cells or may have identified genes with a specialized function in transformed cells. In particular, steps controlling progression through G1 and entry into S phase are largely dependent on the cell type and context[9]. Many of the genes uncovered in this category may therefore be specific for HeLa cells, and a knockdown in a different cell line may produce a different phenotype. In addition, many of the reported genes causing a G0/G1 arrest are probably required for cell growth or stress response, with no direct function in cell cycle regulation or progression. In contrast to G1 progression and G1/S transition, mitosis and cytokinesis follow canonical steps that should vary little from cell line to cell line. Hence, many genes identified in this category may be newly identified participants that will also be important for cell division in most mammalian cells. Thus, the large number of newly described gene functions from this study will be a rich starting point for future work in research on the cell cycle and cancer.

We have demonstrated the potential of phenotypic RNAi profiling in assigning potential functions to novel genes and multiprotein complexes in combination with bioinformatics, cross-species comparisons and mining of proteomic data. This was highlighted by the identification of two putatively conserved transcriptional networks governing cytokinesis. For model organisms with genome-wide data sets of protein interactions such as *C. elegans*, the power of this approach for the identification of functional modules has recently been demonstrated[41]. We therefore expect that the comparative analysis of large-scale RNAi data sets with the growing number of interaction data for mammalian proteomes[42] will facilitate the identification of additional functional networks governing mammalian cell division. □

METHODS

Generation of a genome-scale esiRNA library. esiRNAs were synthesized as described previously[13,43]. Normalized esiRNAs were arrayed into 384-well plates for genome-scale screening.

Cell-based screening. esiRNAs (15 ng) were reversely transfected with Oligofectamine (Invitrogen, Karlsruhe, Germany) in 384-well tissue culture plates (Greiner, Frickenhausen, Germany). For DNA content analysis, the cells were fixed and stained with propidium iodide (Molecular Probes, Leiden, The Netherlands) and scanned with an Acumen Explorer microplate cytometer (TTP LabTech, Melbourn, UK). The resulting DNA-content histograms were manually gated with the Acumen Explorer software (TTP LabTech) to quantify the cell number and the percentages of cells with subG1, G1, S, G2/M phase, $4N–8N$ and $8N$ DNA content.

For determination of the mitotic index the cells were fixed and incubated with primary antibodies against tubulin (Serotec, Dusseldorf, Germany), phospho-histone H3 (Cell Signaling, Danvers, MA) and pericentrin (Abcam, Cambridge, UK) and subsequently with the secondary antibodies donkey anti-mouse Alexa 647, donkey anti-rabbit Alexa 555 and donkey anti-rat Alexa 488 secondary antibodies at 0.4 μg ml^{−1} (Molecular Probes) and 1 μg ml^{−1} 4′,6-diamidino-2-phenylindole (DAPI; Sigma, Taufkirchen, Germany). Images were acquired on the CellWoRx system (Applied Precision, issaquah, WA) and the mitotic index was calculated automatically.

For measurement of cell size we used the forward scatter determined by fluorescence-activated cell sorting analysis of detached cells with a FACSCalibur (BD Biosciences, Heidelberg, Germany) using CellQuestPro software.

Hit selection and validation; clustering analyses. Each determined parameter was normalized for each well by using the mean and s.d. of eight negative controls (esiRNAs targeting firefly and *Renilla* luciferase) for an individual 384-well plate. We scored hits in the primary screen when the averages for the G1, S, G2M phase, or polyploid DNA content were greater than 3, indicating statistically highly significant hits.

To minimize the number of false positives in our screen we validated the primary hits, for which we considered two major sources of false positives: first, experimental errors, and second, off-target effects caused by the knockdown of unintended transcripts. To exclude these false positives from our primary hit list we performed three consecutive analyses. First, we analysed the expression status of the primary hits in HeLa cells. We reasoned that true positives must be expressed in HeLa cells whereas primary hits that are not expressed probably represent false positives. We therefore performed RT–PCR for the primary hits for complementary DNA prepared from the HeLa cells or *in silico* analysis of microarray data (see Supplementary Methods) and found that 1,748 out of 1,964 (89%) of the tested primary hits were expressed. Second, to eliminate experimental errors, we resynthesized esiRNAs for these genes and repeated the DNA content analysis. We reasoned that phenotypes resulting from experimental errors should not be reproducible in an independent experiment using the original esiRNA as silencing trigger. We were able to reproduce 78% of 1,726 tested initial phenotypes, yielding 1,351 candidate genes (Supplementary Information, Table S1). Third, we generated a second non-overlapping esiRNA for 1,254 of the primary hits to target the same transcript and tested their effect using the DNA content assay. For the remaining 97 genes the design of second esiRNAs was not possible. Using this approach we were able to validate 743 cell cycle arrest/cell division defect phenotypes (59%) in HeLa cells (Supplementary Information, Table S1). The cumulative validation procedure used here therefore ensures that the data set presented here is of high quality and contains a limited number of false positives.

Hierarchical clustering of the 1,351 phenotypic profiles was performed with EPCLUST (http://ep.ebi.ac.uk/EP/EPCLUST) using correlation-measure-based
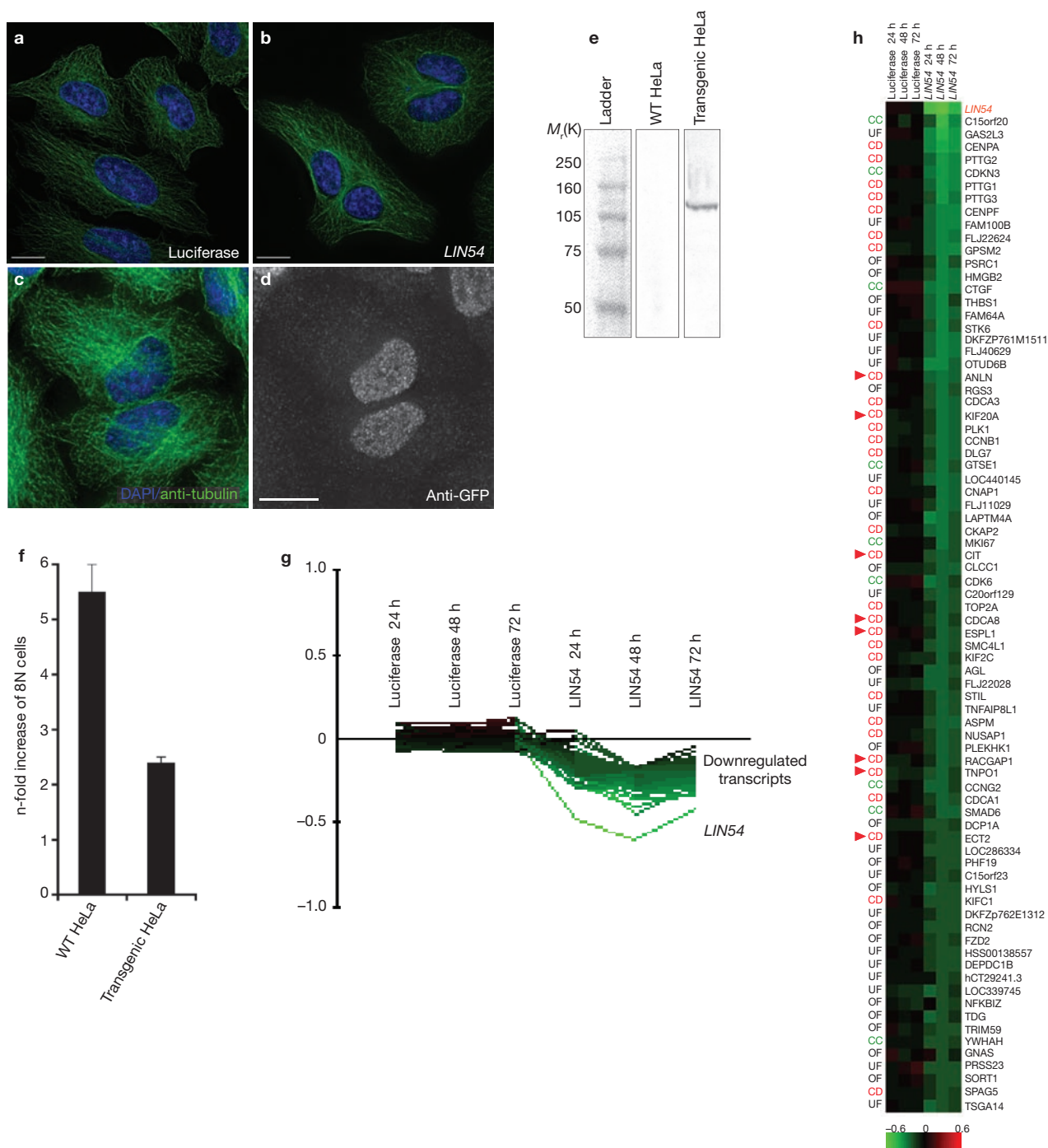
Figure 6 Characterization of LIN54 function in cell division. (**a**, **b**) Cytokinesis defect of LIN54 depletion. HeLa cells were transfected with esiRNA targeting firefly luciferase (**a**) as negative control and LIN54 (**b**) and were imaged by three-dimensional deconvolution microscopy 72 h after transfection for tubulin (green) and DNA (blue). Note the occurrence of binucleate cells on *LIN54* knockdown. (**c–e**) Characterization of LIN54–GFP. HeLa cells containing the mouse LIN54 BAC tagged with GFP stained for DNA (blue) and microtubules (green) (**c**), and GFP (**d**). Scale bars, 10 μm. (**e**) Western blot of wild-type (WT) and transgenic HeLa cell lysates with an anti-GFP antibody shows the presence of the tagged protein with the predicted relative molecular mass of 110,000. (**f**) Cross-species rescue of the cytokinesis defect. Wild-type HeLa cells or HeLa cells stably expressing the mouse LIN54–GFP were subjected to *LIN54*

and luciferase RNAi. At 72 h after transfection, the increase in octaploid (8N) cells compared with the negative control was determined. Error bars represent s.d. *P* was calculated as 0.0008 (*n* = 4) with a two-tailed *t*-test based on a nearly normal distribution of the 8N DNA content for the negative controls in the screen (data not shown). (**g**, **h**) Downregulated transcripts on knockdown of *LIN54*. At 24, 48 and 72 h after transfection of *LIN54* and luciferase esiRNA, RNA was isolated and subjected to microarray analysis. A total of 78 genes with significantly decreased transcript levels (*P* < 0.01, at least 1.5-fold change after 48 h) are shown in a line diagram (**g**) and a heatmap (**h**). Genes causing cytokinesis defects when silenced in our screen are indicated with red arrowheads. Genes are annotated as follows: CC, known cell cycle function; OF, other function; UF, unknown function.

distances and average linkage clustering. As input for EPCLUST we used the averaged normalized values of the nine determined parameters that were cut off at +20 and −20.

Time-lapse microscopic assay. Transfections were performed as described above with a HeLa cell line stably expressing histone–GFP. Time-lapse fluorescence microscopy for 68 cell division defects was performed with a ScanR system (Olympus, Hamburg, Germany). For high-resolution time-lapse imaging, HeLa cells stably expressing histone–GFP were grown and transfected in eight-well LAB-TEK II chambered coverglasses (Nalge Nunc International, Weisbaden-Biebrich, Germany). Cells were imaged 48 h after transfection on a DeltaVision RT system (Applied Precision) and a CoolSnap HQ charge-coupled device (CCD) camera (Roper Scientific, Tucson, AZ).

Immunofluorescence and microscopy for CASC5 and LIN54 phenotypes. Cells were transfected with esiRNAs targeting LIN54 and CASC5 (for esiRNA target sequences see Supplementary Information, Table S1). Cells grown on coverslips were fixed in ice-cold methanol at −20 °C for 5–8 min. After being blocked in 0.2% gelatin from cold-water fish (Sigma) in PBS (PBS/FSG) for 15–30 min, coverslips were incubated for 30 min with primary antibodies in PBS/FSG at the following concentrations: 1:1,000 rat anti-α-tubulin (Serotec); 1:1,000 mouse anti-hBub1 (Immuquest, Seamer, UK); 1:1,000 mouse anti-hBubR1 (Immuquest); 1:500 human anti-CREST (Europa Bioproducts Ltd, Cambridge, UK) or 1:1,000 sheep anti-GFP. After washes with 0.2% PBS/FSG, cells were incubated with 1:500 dilution of secondary antibodies for 30 min (donkey anti-mouse, rabbit, rat or sheep conjugated to Alexa 488, Alexa 594, Alexa 647; Molecular Probes). Coverslips were counterstained with 1 μg ml⁻¹ DAPI to visualize chromatin. After being washed with 0.2% FSG/PBS, coverslips were mounted on glass slides by inverting them into mounting solution. Three-dimensional image datasets were acquired on an imaging system (DeltaVision; Applied Precision) equipped with a microscope (model IX71; Olympus), a CCD camera (CoolSNAP HQ2 1,024 × 1,024; Roper Scientific), and 60×, numerical aperture 1.42, plan-Apochromat objectives using 1 × 1 binning. Z-stacks (35 sections, 0.2 μm apart for each optical section) were collected and deconvolved computationally with the SoftwoRx software package (v3.6; Applied Precision).

Tagging of bacterial artificial chromosomes (BACs). The BACs RP23-96B7 (harbouring *mLIN54*) and RP23-428F16 (harbouring *mPCNA*), were obtained from the BACPAC Resources Center (http://bacpac.chori.org). A localisation and affinity purification (LAP) cassette[44] was inserted as a carboxy-terminal fusion using recombineering. Isolated BAC DNA was transfected and selected for stable integration as described[31].

Western blotting. Whole-cell lysates of 100,000 cells stably transfected with mLIN54-LAP were subjected to SDS–PAGE (NuPage 4–12% Bis-Tris; Invitrogen), blotted, and subsequently incubated with an anti-GFP antibody (1:5,000 dilution; Roche, Mannheim, Germany). After incubation with anti-mouse IgG conjugated with horseradish peroxidase (Bio-Rad, Munich, Germany), bands were detected with enhanced chemiluminescence (ECL) Western Blotting Detection Reagents (Amersham, Piscataway, NJ). As a ladder, Full-Range Rainbow Molecular Weight Marker (10–250 kDa; RPN800; Amersham) was used.

Microarray experiments. RNA isolated from esiRNA-transfected cells was hybridized against RNA from mock-transfected cells. Transfection, total RNA purification and processing, microarray hybridization and analyses were performed as described previously[13].

A more detailed description of the experimental procedures and data analysis is provided in Supplementary Methods.

Accession number. Gene Expression Omnibus (GEO): GSE9176.

Note: Supplementary Information is available on the Nature Cell Biology website.

AUTHOR CONTRIBUTIONS
R.K and L.P. contributed equally to this work. R.K., L.P. and F.B. performed project planning, experimental work and data analysis. A.-K.H., M.S., M.T., L.M., I.P., S.L., H.G., K.K., J.W., V.S., C.R., W.B., A.L.J. and B.H. performed experimental work and data analysis. A.A.H. performed data analysis.

1. Hannon, G. J. RNA interference. *Nature* **418,** 244–251 (2002).
2. Echeverri, C. J. & Perrimon, N. High-throughput RNAi screening in cultured cells: a user's guide. *Nature Rev. Genet.* **7,** 373–384 (2006).
3. Bjorklund, M. *et al.* Identification of pathways regulating cell size and cell-cycle progression by RNAi. *Nature* **439,** 1009–1013 (2006).
4. Eggert, U. S. *et al.* Parallel chemical genetic and genome-wide RNAi screens identify cytokinesis inhibitors and targets. *PLoS Biol.* **2,** e379 (2004).
5. Bettencourt-Dias, M. *et al.* Genome-wide survey of protein kinases required for cell cycle progression. *Nature* **432,** 980–987 (2004).
6. Gonczy, P. *et al.* Functional genomic analysis of cell division in *C. elegans* using RNAi of genes on chromosome III. *Nature* **408,** 331–336 (2000).
7. Sönnichsen, B. *et al.* Full-genome RNAi profiling of early embryogenesis in *Caenorhabditis elegans. Nature* **434,** 462–469 (2005).
8. Kastan, M. B. & Bartek, J. Cell-cycle checkpoints and cancer. *Nature* **432,** 316–323 (2004).
9. Massagué, J. G1 cell-cycle control and cancer. *Nature* **432,** 298–306 (2004).
10. Rajagopalan, H. & Lengauer, C. Aneuploidy and cancer. *Nature* **432,** 338–341 (2004).
11. Buchholz, F., Kittler, R., Slabicki, M. & Theis, M. Enzymatically prepared RNAi libraries. *Nature Methods* **3,** 696–700 (2006).
12. Kittler, R. *et al.* An endoribonuclease-prepared siRNA screen in human cells identifies genes essential for cell division. *Nature* **432,** 1036–1040 (2004).
13. Kittler, R. *et al.* Genome-wide resources of endoribonuclease-prepared short interfering RNAs for specific loss-of-function studies. *Nature Methods* **4,** 337–344 (2007).
14. Jackson, A. L. *et al.* Expression profiling reveals off-target gene regulation by RNAi. *Nature Biotechnol.* **21,** 635–637 (2003).
15. Birmingham, A. *et al.* 3′ UTR seed matches, but not overall identity, are associated with RNAi off-targets. *Nature Methods* **3,** 199–204 (2006).
16. Jackson, A. L. *et al.* Widespread siRNA 'off-target' transcript silencing mediated by seed region sequence complementarity. *RNA* **12,** 1179–1187 (2006).
17. Nelson, D. M. *et al.* Coupling of DNA synthesis and histone synthesis in S phase independent of cyclin/cdk2 activity. *Mol. Cell. Biol.* **22,** 7459–7472 (2002).
18. Ye, X. *et al.* Defective S phase chromatin assembly causes DNA damage, activation of the S phase checkpoint, and S phase arrest. *Mol. Cell* **11,** 341–351 (2003).
19. Shiomi, Y. *et al.* ATP-dependent structural change of the eukaryotic clamp-loader protein, replication factor C. *Proc. Natl Acad. Sci. USA* **97,** 14127–14132 (2000).
20. Storchova, Z. & Pellman, D. From polyploidy to aneuploidy, genome instability and cancer. *Nature Rev. Mol. Cell Biol.* **5,** 45–54 (2004).
21. Takimoto, M. *et al.* Frequent expression of new cancer/testis gene D40/AF15q14 in lung cancers of smokers. *Br. J. Cancer* **86,** 1757–1762 (2002).
22. Chinwalla, V. *et al.* A t(11;15) fuses MLL to two different genes, AF15q14 and a novel gene MPFYVE on chromosome 15. *Oncogene* **22,** 1400–1410 (2003).
23. Kuefer, M. U. *et al.* Characterization of the MLL partner gene AF15q14 involved in t(11;15)(q23;q14). *Oncogene* **22,** 1418–1424 (2003).
24. Cheeseman, I. M. *et al.* A conserved protein network controls assembly of the outer kinetochore and its ability to sustain tension. *Genes Dev.* **18,** 2255–2268 (2004).
25. Obuse, C. *et al.* A conserved Mis12 centromere complex is linked to heterochromatic HP1 and outer kinetochore protein Zwint-1. *Nature Cell Biol.* **6,** 1135–1141 (2004).
26. Desai, A. *et al.* KNL-1 directs assembly of the microtubule-binding interface of the kinetochore in *C. elegans. Genes Dev.* **17,** 2421–2435 (2003).
27. Mukherji, M. *et al.* Genome-wide functional analysis of human cell-cycle regulators. *Proc. Natl Acad. Sci. USA* **103,** 14819–14824 (2006).
28. Echard, A., Hickson, G. R., Foley, E. & O'Farrell, P. H. Terminal cytokinesis events uncovered after an RNAi screen. *Curr. Biol.* **14,** 1685–1693 (2004).
29. Jepsen, K. & Rosenfeld, M. G. Biological roles and mechanistic actions of co-repressor complexes. *J. Cell Sci.* **115,** 689–698 (2002).
30. Pijnappel, W. W. *et al.* The *S. cerevisiae* SET3 complex includes two histone deacetylases, Hos2 and Hst1, and is a meiotic-specific repressor of the sporulation gene program. *Genes Dev.* **15,** 2991–3004 (2001).
31. Kittler, R. *et al.* RNA interference rescue by bacterial artificial chromosome transgenesis in mammalian tissue culture cells. *Proc. Natl Acad. Sci. USA* **102,** 2396–2401 (2005).
32. Lewis, P. W. *et al.* Identification of a *Drosophila* Myb-E2F2/RBF transcriptional repressor complex. *Genes Dev.* **18,** 2929–2940 (2004).

33. Korenjak, M. *et al.* Native E2F/RBF complexes contain Myb-interacting proteins and repress transcription of developmentally controlled E2F target genes. *Cell* **119,** 181–193 (2004).

34. Harrison, M. M., Ceol, C. J., Lu, X. & Horvitz, H. R. Some *C. elegans* class B synthetic multivulva proteins encode a conserved LIN-35 Rb-containing complex distinct from a NuRD-like complex. *Proc. Natl Acad. Sci. USA* **103,** 16782–16787 (2006).

35. Dimova, D. K., Stevaux, O., Frolov, M. V. & Dyson, N. J. Cell cycle-dependent and cell cycle-independent control of transcription by the *Drosophila* E2F/RB pathway. *Genes Dev.* **17,** 2308–2320 (2003).

36. Ren, B. *et al.* E2F integrates cell cycle progression with DNA repair, replication, and G$_2$/M checkpoints. *Genes Dev.* **16,** 245–256 (2002).

37. Hauser, B. A., He, J. Q., Park, S. O. & Gasser, C. S. TSO1 is a novel protein that modulates cytokinesis and cell expansion in *Arabidopsis. Development* **127,** 2219–2226 (2000).

38. Beall, E. L. *et al.* Role for a *Drosophila* Myb-containing protein complex in site-specific DNA replication. *Nature* **420,** 833–837 (2002).

39. Litovchick, L. *et al.* Evolutionarily conserved multisubunit RBL2/p130 and E2F4 protein complex represses human cell cycle-dependent genes in quiescence. *Mol. Cell* **26,** 539–551 (2007).

40. Echeverri, C. J. *et al.* Minimizing the risk of reporting false positives in large-scale RNAi screens. *Nature Methods* **3,** 777–779 (2006).

41. Gunsalus, K. C. *et al.* Predictive models of molecular machines involved in *Caenorhabditis elegans* early embryogenesis. *Nature* **436,** 861–865 (2005).

42. Rual, J. F. *et al.* Towards a proteome-scale map of the human protein–protein interaction network. *Nature* **437,** 1173–1178 (2005).

43. Kittler, R., Heninger, A. K., Franke, K., Habermann, B. & Buchholz, F. Production of endoribonuclease-prepared short interfering RNAs for gene silencing in mammalian cells. *Nature Methods* **2,** 779–784 (2005).

44. Cheeseman, I. M. & Desai, A. A combined approach for the localization and tandem affinity purification of protein complexes from metazoans. *Sci STKE* **2005,** pl1 (2005).